

## The Green Approach of Cerium Oxide Nanoparticle and Its Application for Photo-degradation of Phenol Dye

Gusliani Eka Putri<sup>1\*</sup>, Syukri Arief<sup>2</sup>, Ahmad Hafizullah Ritonga<sup>3</sup>, Wiya Elsa Fitri<sup>4</sup>, Eliza Arman<sup>1</sup>, Arniat Christiani Telaumbanua<sup>1</sup>, and Rahmi Novita Yusuf<sup>1</sup>

<sup>1</sup>Department of Medical Laboratory Technology, Sekolah Tinggi Ilmu Kesehatan Syedza Saintika, Jl. Prof. Dr. Hamka No. 228, Padang 25132, Indonesia

<sup>2</sup>Department of Chemistry, Faculty of Mathematics and Natural Sciences, Andalas University, Limau Manis Campus, Padang 25163, Indonesia

<sup>3</sup>Institut Kesehatan Medistra Lubuk Pakam, Jl. Sudirman No. 38, Deli Serdang 20512, Indonesia

<sup>4</sup>Department of Public Health, Sekolah Tinggi Ilmu Kesehatan Syedza Saintika, Jl. Prof. Dr. Hamka No. 228, Padang 25132, Indonesia

---

\* **Corresponding author:**

email: guslianiekaputri@gmail.com

Received: January 25, 2023

Accepted: September 28, 2023

DOI: 10.22146/ijc.81657

**Abstract:** The approach to the synthesis of cerium oxide nanoparticles (CeO<sub>2</sub>NPs) using plants as capping agents has been widely researched because of its eco-friendly, low-cost, simple, effective, and reusability. In this research, we used Moringa oleifera leaf extract-mediated CeO<sub>2</sub>NPs. CeO<sub>2</sub>NPs were characterized by XRD, FTIR, SEM, TEM, and DRS UV-vis. The photocatalytic activity of CeO<sub>2</sub>NPs was tested using a phenol dye concentration of 7 mg/L with variations in photocatalyst weight of 10, 20, 30, 40, 50, 60, 70, 80, 90, and 100 mg under UV irradiation, respectively, with time variations of 15, 30, 45, 60, 75, 90, 105, 120, 135, and 150 min. SEM and TEM morphology results showed that the CeO<sub>2</sub>NPs were spherical and agglomerated. The crystal structure is cubic, with a crystal size of 18 nm with a band gap of 2.87 eV. CeO<sub>2</sub>NPs showed high photo-degradation phenol dye of 94.45% under visible light in 120 min irradiation time. The results show that M. oleifera leaf extract could be as inexpensive and safe for synthesizing other metal oxide nanoparticles, potentially having applications in the biomedical and environmental fields.

**Keywords:** cerium oxide nanoparticles; approach synthesis; phenol; Moringa oleifera; photocatalytic

---

### ■ INTRODUCTION

Medical waste contains many chemical compounds that harm humans and the environment [1-2]. Phenol dye is one of the hazardous chemicals in medical waste [3-5]. Based on the Decree of the Environment Ministry of Indonesia Republic No. 51, concentrations of phenol according to quality standards shall be in a range of 0.5–1.0 mg/L. Phenol concentration above the quality standard can cause effects on humans, including liver and kidney damage, decreased blood pressure, weakened heart rate, and even death [6-7].

Central General Hospital Dr. M. Djamil Padang is the largest type A hospital in West Sumatra. Based on this condition, many patients' treatment will increase the amount of liquid waste produced, including phenolic compounds. Conventional methods that have been applied to decompose phenol wastes are steam distillation [8], liquid-liquid extraction [9], solid-phase extraction [10], and biodegradation [11]. In the last decade, many studies have proven that photocatalyst technology is better at degrading organic compounds; thus, it is more economical in energy use and can reduce the use of chemicals [12].

Photocatalyst processes usually use metals and metal oxides such as  $\text{TiO}_2$  [13-14],  $\text{ZnO}$  [15], and  $\text{Ag}$  [16]. However, the use of this metal in the degradation of phenol waste still gets a percentage of phenol waste under 50%, and optimal conversion data for phenolic waste has yet to be obtained. So, in recent years, many researchers have been interested in using cerium oxide ( $\text{CeO}_2$ ) as a photocatalyst.  $\text{CeO}_2$  is a semiconductor with a 3.0–3.9 eV band gap in bulk, chemical stability, thermal stability, and high conductivity that can absorb UV light and has catalytic and optical properties [17-18]. Various fields of application, such as UV absorbers [19], biosensors [20], sunscreens cosmetics [21], biomedical applications [22], and photo-catalysts [23], have been reported.  $\text{CeO}_2$  nanoparticles ( $\text{CeO}_2\text{NPs}$ ) act as heterogeneous catalysts [24], so they easily separate from the waste after the photocatalyst process is completed so as not to harm the environment [25].

The synthesis of the  $\text{CeO}_2\text{NPs}$  had previously been used utilizing chemical substances such as acids (acetic acid) or bases (ammonium hydroxide) [26]. Various leaf extracts from plants have been used in the green synthesis of  $\text{CeO}_2\text{NPs}$ , including *Gloriosa superba* leaf extract [27], *Olei europaea* leaf extract [28], *Prosopis juliflora* leaf extract [29], and *Calotropis procera* flower extract [30]. In this study, *Moringa oleifera* leaf extract was used to perform green synthesis of  $\text{CeO}_2\text{NPs}$ . A literature search revealed that no prior work has used this extract to create  $\text{CeO}_2\text{NPs}$ . Phytochemical testing of *M. oleifera* leaf extract contains flavonoids, triterpenoids, steroids, saponins, and tannins. They act as capping agents in the process of synthesis of nanoparticles. The usage of this technique is more environmentally beneficial because it does not use harmful chemicals in nanoparticle synthesis [17,31].

The increased phenol content in wastewater has forced dye manufacturers to address their environmental impact. Conventional chemical methods do not effectively decompose phenol into innocuous byproducts, according to prior studies. This situation became the main reason for the scientific community to develop new effective processes for the decomposition of phenol dye. Due to its affordability, environmental friendliness, and simplicity in process control, photocatalytic techniques

have attracted the attention of numerous phenol degradation researchers [32].

For the development of  $\text{CeO}_2\text{NPs}$  in the degradation of phenol under visible light irradiation, *M. oleifera* potential reduction agents and stabilizing activity may be utilized as a suitable green synthesis method. Based on research gaps, the present research showed the potential activity reduction and stabilization agent of *M. oleifera* extract for the photosynthesis of  $\text{CeO}_2\text{NPs}$ . According to related literature, there have not been any investigations into the photocatalytic activity of  $\text{CeO}_2\text{NPs}$  mediating *M. oleifera* for phenol degradation.

## ■ EXPERIMENTAL SECTION

### Materials

The materials used in this study were *M. oleifera* leaves from *Balai Benih Induk Tanaman* (Center for Mother Plant Seed) at Lubuk Minturun, Koto Tangah, Padang, West Sumatra, Indonesia. Sigma-Aldrich offered phenol with a 99% purity and cerium nitrate hexahydrate ( $\text{Ce}(\text{NO}_3)_3 \cdot 6\text{H}_2\text{O}$ ) with a 99.99% purity.

### Instrumentation

The powder X-ray diffractogram (XRD) of synthesized and calcined samples was recorded on a Rigaku Miniflex diffractometer with  $\text{Cu-K}\alpha$  radiation between 20 and 90° ( $2\theta$ ) with a scanning rate of 1°/min. TEM micrographs of the samples were obtained with a JEOL 100CX microscope with 100 kV of acceleration voltage. SEM using the JEOL-JSM 6360 LA.

### Procedure

#### **Synthesis of $\text{CeO}_2\text{NPs}$**

*M. oleifera* were collected from the Balai Benih Induk Tanaman (Center for Mother Plant Seed) and taxonomic identification was carried out in Herbarium Universitas Andalas (ANDA), Andalas University, Padang, Indonesia. Secondary metabolites were identified at the Laboratory of Natural Products, Chemistry Department, Andalas University. The leaves were shade-dried at room temperature for about 5 d, and the dried leaves were then mashed up to obtain a fine powder. As much as 10 g of *M. oleifera* leaf powder was dissolved in 50 mL double distilled water for 30 min at 65 °C. The

obtained extract was filtered with Whatman No.1 filter paper and stored in a sealed bottle at 4 °C for further use.

Ce(NO<sub>3</sub>)<sub>3</sub>·6H<sub>2</sub>O (0.1 mol) was added to 200 mL of *M. oleifera* leaf extract and stirred at a speed of 500 rpm at a temperature of 80 °C for 2 h. The solution was filtered, washed with distilled water, and dried in an oven at 80 °C for 4 h. CeO<sub>2</sub> was synthesized in a furnace at 600 °C for 2 h [2].

### Degradation of phenol dye

Photocatalytic degradation was carried out at room temperature using a batch photo-reactor setup. The photocatalytic activity of CeO<sub>2</sub>NPs is used to decompose phenol with known concentrations. The six beaker glasses were wrapped in black plastic, each with 250 mL of phenol, and added with the CeO<sub>2</sub> photocatalyst (0, 10, 20, 30, 40, 50, 60, 70, 80, 90, and 100 mg). The beaker glasses were put into a radiation box and wrapped with the new black plastic. Next, the beaker glasses were irradiated with a visible 300 W Xenon lamp (Cermax® Xenon, Excelitas, USA) with a wavelength (λ) > 400 nm with time variations for 15, 30, 45, 60, 75, 90, 105, and 120 min. After the radiation process, the suspension from each beaker glass was centrifuged. The absorbance of the supernatant was measured with a UV-vis spectrophotometer at the maximum length of phenol.

## RESULTS AND DISCUSSION

The concentration phenol of medical waste from Central General Hospital (RSUP) Dr. M. Djamil Padang was analyzed in the Chemistry Laboratory, Medical Laboratory Technology Department, STIKES Syedza Saintika. The analyzed parameters were the concentration of phenol and pH measurement using a spectrophotometer and pH meter. It can be shown in Table 1 according to the standard based on Minister of Environment Regulation of the Republic of Indonesia No. 5 of 2014 on "Wastewater Quality Standards".

The phenolic concentration in a liquid waste sample in the initial reservoir before processing is 6.65 mg/L with pH 8, then used to make an artificial phenol solution become 7 mg/L. This research used CeO<sub>2</sub> as a photocatalyst with variations in the weight and degradation time.

### Nanoparticle Characterization

The aim of XRD characterization is to know the crystal structure. The specific peaks of CeO<sub>2</sub> at 2θ 28.83, 32.82, 47.34, 56.71, 69.96, and 76.66, respectively, represent for hkl (111), (200), (220), (311), (400), and (420), as shown in Fig. 1(a). The CeO<sub>2</sub>NPs have a cubic structure according to ICPDS Card No. 34-0394. This spectrum showed no impurity peaks, which confirmed that single-phase CeO<sub>2</sub> crystals were successively formed. The strong crystallinity of CeO<sub>2</sub>NPs and spectrum diffraction peak was narrow with a crystal size calculated using the Debye-Scherrer equation (Eq. (1)).

$$D = \frac{\lambda}{\beta \cos \theta} \quad (1)$$

Here, the full width at half maximum (FWHM) value is β, the diffraction angle is θ, the size of the crystallite is D, the numerical factor corresponding to the crystallite shape factor is K, and the wavelength of X-ray is λ [30].

**Table 1.** The chemical parameters in the hospital waste

Parameters	Unit	Sample	The wastewater quality standard*
Phenol	mg/L	6.65	0.50–1.00
pH	mg/L	8.0	6.0–9.0

\*based on Minister of Environment Regulation of the Republic of Indonesia No. 5 of 2014

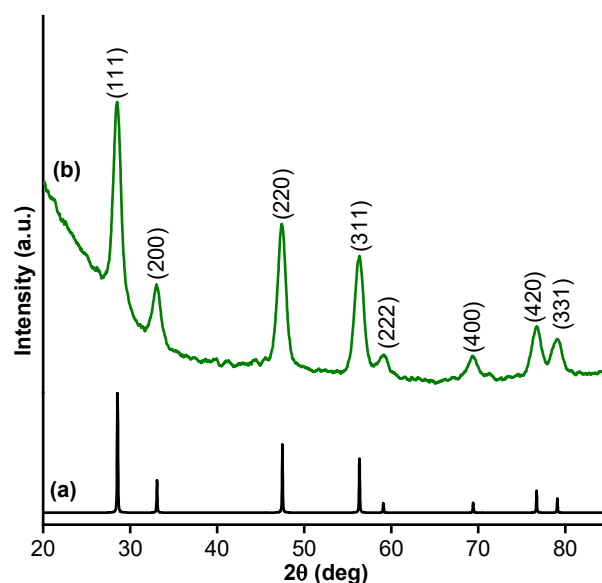


**Fig 1.** XRD profile of (a) standard of CeO<sub>2</sub> (ICSD-34-0394) (b) as-synthesized CeO<sub>2</sub>NPs

It became known that the average crystallite size of  $\text{CeO}_2$ NPs produced using *M. oleifera* leaf extract was 28 nm.

Fig. 2 shows the  $\text{CeO}_2$ NPs FTIR spectrum. The KBr pellet method was applied to conduct the FTIR study, which was scanned in the  $400\text{--}4000\text{ cm}^{-1}$  wavelength range. The absorption bands at  $1300$ , around  $1600$ , and  $3300\text{ cm}^{-1}$  are referred to as N-O stretching, H-O-H bond, and OH stretching in the FTIR spectra of  $\text{CeNO}_3\cdot 6\text{H}_2\text{O}$  respectively (Fig. 2(a)). The FTIR absorption spectrum of  $\text{CeO}_2$ NPs after calcination in Fig. 2(b) shows the intensity of  $453$  and  $685\text{ cm}^{-1}$ , which are referred to  $\text{Ce-O}$  stretching and O-Ce-O bonding, respectively. It was observed that the OH peak of the water appears to be reduced in  $\text{CeO}_2$  form. The results of this study are in line with Arumugam et al. [27], who also found the peak of  $\text{Ce-O}$  stretching to be  $451\text{ cm}^{-1}$ .

The morphology of the nanoparticles was shown from the SEM, TEM, and HRTEM analysis. Fig. 3(a)

morphology analysis that can show the TEM image. It can SEM data show the  $\text{CeO}_2$ NPs morphology where the

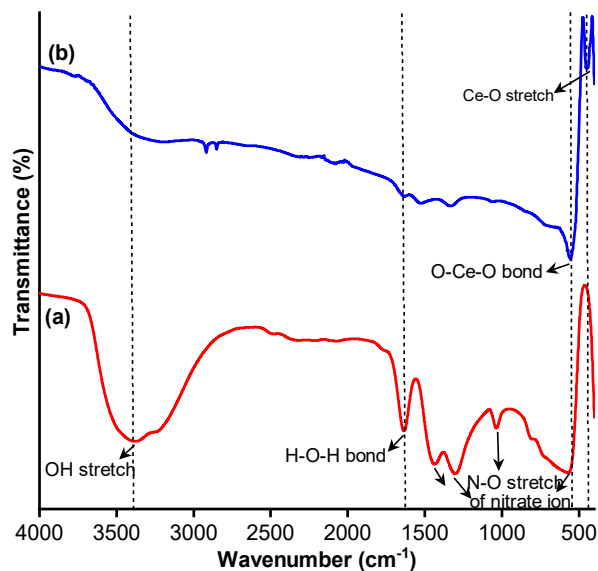


**Fig 2.** FTIR spectra of (a)  $\text{CeNO}_3\cdot 6\text{H}_2\text{O}$  precursor (b) as-synthesized  $\text{CeO}_2$ NPs

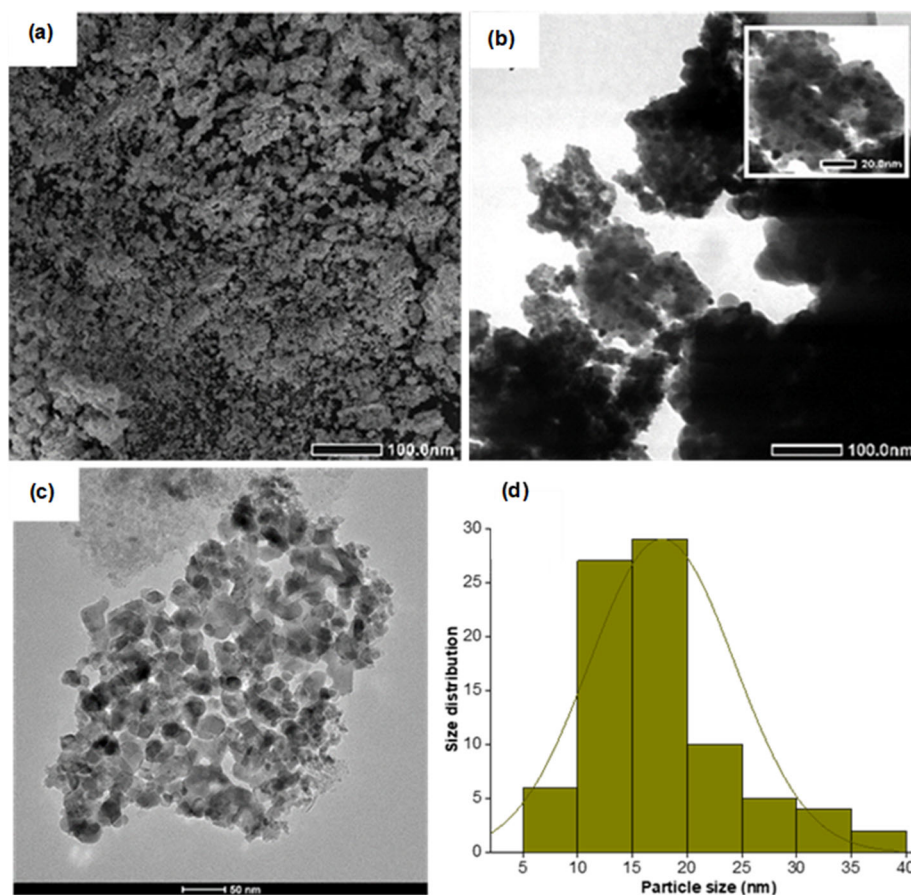


**Fig 3.** (a) SEM, (b) TEM, (c) HR TEM, and (d) size distribution diagram of as-synthesized  $\text{CeO}_2$ NPs

particles are agglomerated. Fig. 3(b) is a microstructural be shown that the particles are spherical and agglomerated. The clear microstructural morphology analysis can be shown in HRTEM data in Fig. 3(c). Particle size was calculated using the Image J application from HRTEM image data and obtained a particle size of 5–40 nm, with a mean particle size of 18 nm described in the histogram in Fig. 3(d).

The Kubelka-Munk equation (Eq. (2)), which has the following formula, was used to compute the amount of absorption whereas  $F(R)$  is known as the Kubelka-Munk function,  $K$  is the molar absorbance coefficient,  $S$  is the scattering factor,  $R$  is the material's reflectance value.

$$F(R) = \frac{K}{S} = \frac{(1-R)^2}{2R} \quad (2)$$

Band gap energy obtained from the graph of the relationship between  $h\nu$  (eV) vs  $(F(R)h\nu)^{1/2}$  determined by Eq. (3);

$$E_g = h\nu = \frac{hc}{\lambda} \quad (3)$$

where  $h$  is Planck's constant ( $6.624 \times 10^{-34}$  J s),  $c$  is the speed of light in the air ( $2.998 \times 10^8$  m/s),  $\lambda$  is the wavelength (nm), and  $E_g$  represents the band gap energy (eV). The value of the  $h\nu$  at  $(F(R)h\nu)^{1/2} = 0$ , which is determined by the linear regression equation of the curve [33] (Fig. 4). The band gap of  $\text{CeO}_2$  in its bulk form is relatively large, with values ranging from 3.0 to 3.9 eV.

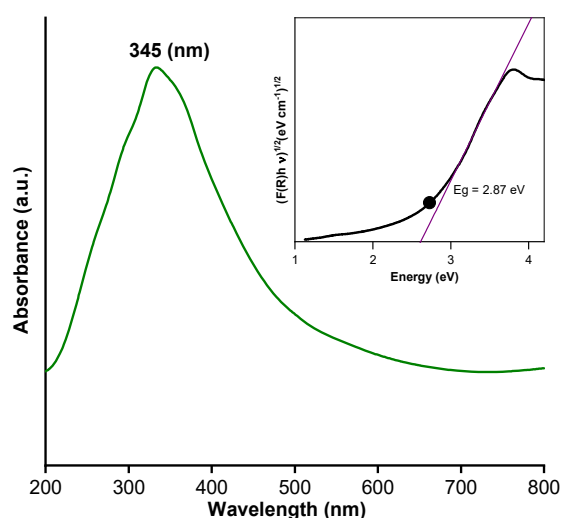


**Fig 4.** DRS UV-vis spectrum of  $\text{CeO}_2$ NPs inserts band gap value of  $\text{CeO}_2$ NPs by Kubelka Munk equation

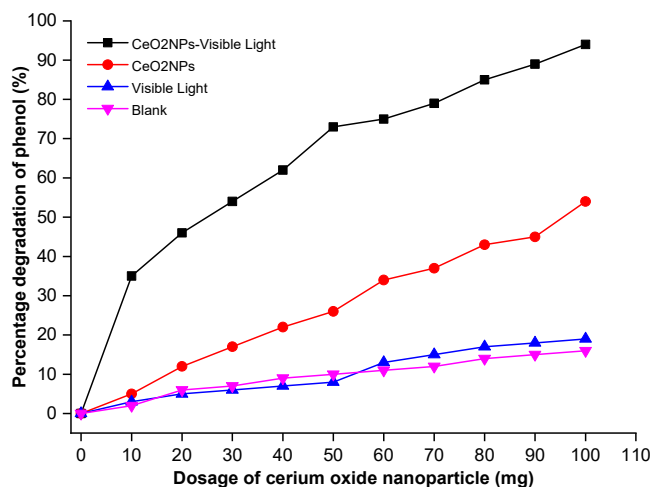
According to preliminary research, a few investigations have reported on reducing the band gap of  $\text{CeO}_2$  without the use of dopants. However, it is frequently applied using harsh techniques at relatively high temperatures. Scott et al. [34] synthesized  $\text{CeO}_2$  NPs with a minimum band gap of 2.73 eV but using a thermal treatment at 600 °C for 4 h to remove the  $\text{CeOHCO}_3$  phase formed during the synthesis process. This research e gab value was 2.87 eV at 600 °C for 2 h. The narrowing of the band gap is achieved thanks to the high structural disorder of the nanoparticles synthesized. The smaller the nanoparticles, the smaller the band gap value. The literature shows the opposite behavior for nanoparticles due to the quantum confinement effect [35]. Additionally, because it causes a change in the strength of attachment of the atoms in the crystalline structure, the structural disorder assists in decreasing the band gap. This information matches XRD results that suggest a crystallite size of 28 nm. The visible region can use a photocatalyst because the energy gap value was 2.87 eV (Fig. 4). The photocatalyst will absorb light with a lower energy level when the gap energy is reduced, but there is a higher chance of electron recombination is greater.

### The Photocatalysis Application

The weight of  $\text{CeO}_2$ NPs was varied at 10, 20, 30, 40, 50, 60, 70, 80, 90, and 100 mg. The degradation time variation of phenol dye using  $\text{CeO}_2$  NPs photocatalyst was 0, 30, 45, 60, 75, 90, 105, and 120 min. The artificial solution volume is 250 mL, and the used time is 100 min with a pH of 8. The result can be seen in Fig. 5 and 6 whereas visible light data refer to the absence of  $\text{CeO}_2$  NPs while blank data refer to the absence of both  $\text{CeO}_2$  NPs and visible light.

Based on Fig. 5 and 6, when the photocatalyst weight is 100 mg, it can decompose 92.45% of the phenol dye, and the removal concentration becomes 0.4 mg/L.

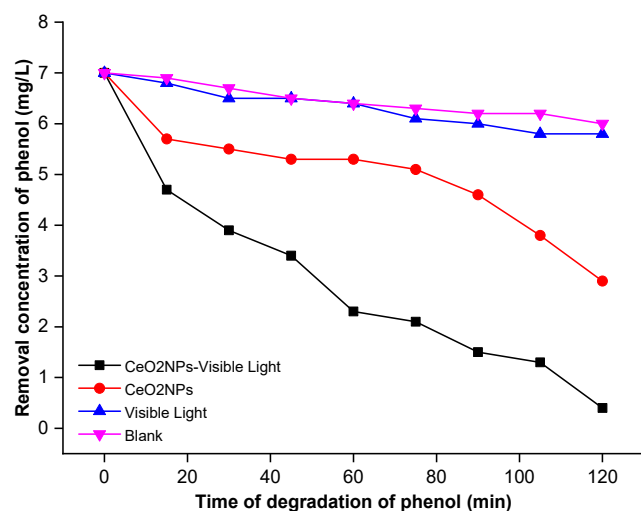
In this study, the phenol dye degradation time variation using  $\text{CeO}_2$ NPs photocatalyst was 0, 30, 45, 60, 75, 90, 105, and 120 min. The volume of the artificial solution is 250 mL, and the mass of the photocatalyst used is 100 mg, with a pH of 8. Respectively,  $\text{CeO}_2$ NPs showed high phenol degradation up to 94.45% at 120 min



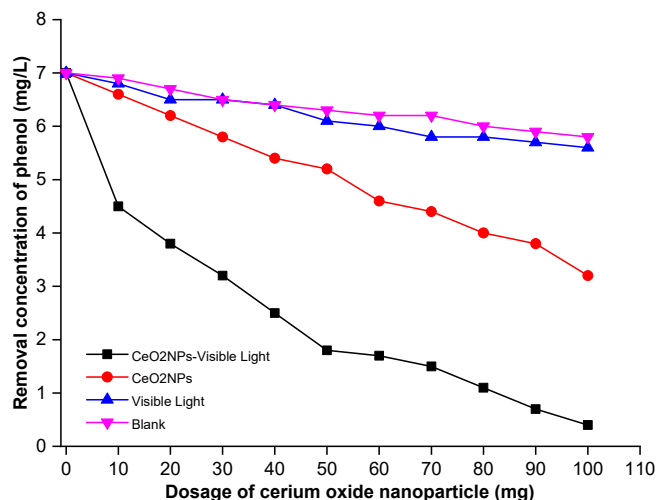
**Fig 5.** The percentage degradation of phenol versus dosage of CeO<sub>2</sub> using visible light irradiation

of irradiation time, as shown in Fig. 7 and 8. CeO<sub>2</sub>NPs show a high degree of photocatalytic activity as a result of photogenerated electron-hole pairs on the photocatalyst surface. It was also comparable to other metal oxide photocatalysts described in the literature and shown in Table 2 when phenol was photocatalytically degraded on the surface of CeO<sub>2</sub>NPs catalysts for photosynthesis in the presence of a visible light source.

The comparison of other metal oxide photocatalysts is shown in Table 2. The activity photo-degradation of CeO<sub>2</sub>NPs synthesized was compared with other literature using metal oxide for phenol degradation.



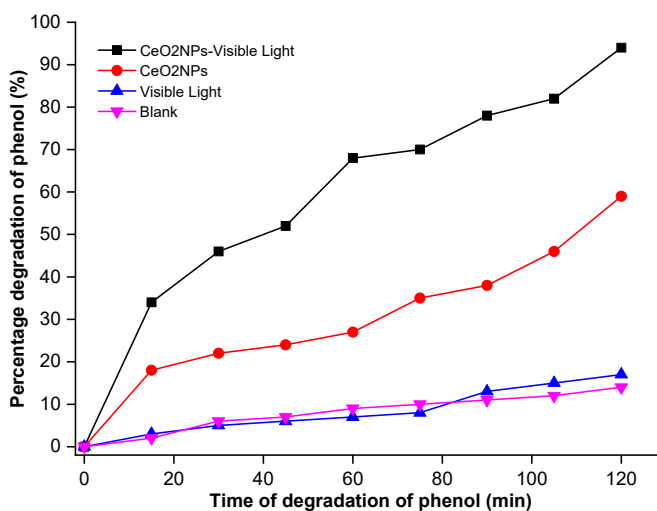
**Fig 7.** The removal concentration of phenol versus irradiation time using visible light irradiation



**Fig 6.** The removal concentration of phenol versus dosage of CeO<sub>2</sub> using visible light irradiation

It can be concluded that metal oxides cause different photo-degradation activities. The photo-degradation activity of CeO<sub>2</sub>NPs in this study was reported in the range of 70–89%. It shows that the CeO<sub>2</sub>NPs photocatalyst synthesized by the green synthesis method can also degrade phenol waste with visible light source irradiation.

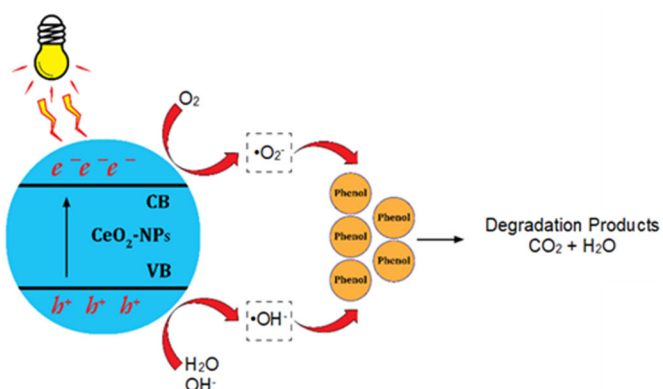
The illustration of the phenol degradation mechanism compounds in the presence of visible light on the surface of CeO<sub>2</sub>NPs is shown in Fig. 9. When the CeO<sub>2</sub>NPs photocatalyst absorbs photon light irradiation, phenol degradation occurs on the surface of



**Fig 8.** The percentage degradation of phenol versus irradiation time using visible light irradiation

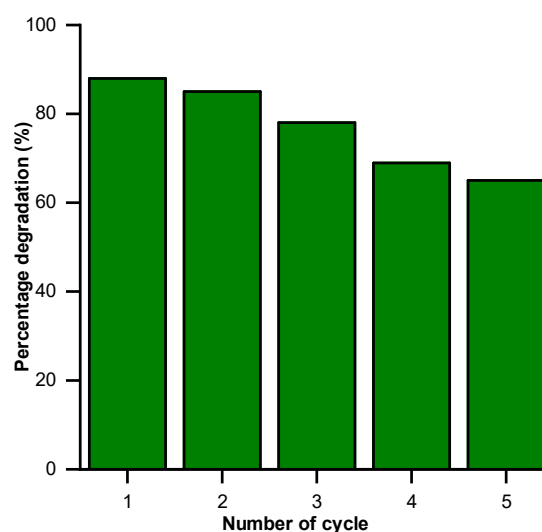
**Table 2.** The comparison of degradation percentages on phenol degradation by metal oxide nanoparticles

Catalyst	Dosage (mg/L)	Time (min)	Percentage degradation rate (%)	Ref.
TiO <sub>2</sub> nanoparticle	150	105	82.00	[36]
Ni nanoparticle	200	120	78.00	[37]
Zirconia nanoparticle	100	150	79.00	[38]
Zinc oxide nanorod	100	180	45.00	[39]
Ag nanoparticle	200	100	89.00	[40]
CeO <sub>2</sub> NPs	100	120	94.45	This work

**Fig 9.** The phenol degradation mechanism

the CeO<sub>2</sub>NPs photocatalyst through superoxide (O<sub>2</sub><sup>-</sup>) radicals and the hydroxyl (OH) radical. According to the degradation mechanism, when the CeO<sub>2</sub>NPs photocatalyst absorbs photon light, electrons jump from the valence band (VB) to the conduction band (CB). Then, holes (h<sup>+</sup>) were formed in VB and electrons (e<sup>-</sup>) in CB. The electron-hole pairs photogenerated onto the surface of the and generated free OH radicals on the CeO<sub>2</sub>NPs surface [41]. It indicates that CeO<sub>2</sub>NPs have a good ability to generate OH radicals in the phenol waste solution. The photogenerated electrons in the CB can generate superoxide radicals. The superoxide radical anion has a significantly more ability to remove pollutants than of OH [2]. Thus, more hole pairs will reach the CeO<sub>2</sub>NPs surface, increasing the phenol degradation.

During photocatalyst reusability under UV light exposure with five recycle uses, the photocatalytic activity of CeO<sub>2</sub>NPs was additionally examined. In the first cycle, the photodegradation efficiency for the phenol dye using CeO<sub>2</sub>NPs was 94.45%. After the first cycle concluded, the CeO<sub>2</sub>NPs were separated by centrifugation, then washed with aquadest and dried for 2 h at 100 °C in an oven. For the subsequent cycle of photodegradation of phenol dye

**Fig 10.** Reusability of CeO<sub>2</sub>NPs for five cycles

under the same conditions, the dried photocatalyst was utilized. Fig. 10 illustrates the CeO<sub>2</sub>NPs' five-cycle recyclability. The recycling study over five cycles, which showed a higher turnover rate and photocatalyst stability, did not substantially impact the photodegradation efficiency of CeO<sub>2</sub>NPs. The photocatalytic activity of CeO<sub>2</sub>NPs showed a dramatically decreased of phenol degradation percentage, probably caused by the material loss during the recovery procedure [38]. In addition, the reduction in surface area during treatment eventually caused the photocatalytic effectiveness to decrease. Because no substantial leaching occurred after seven additional trials, the CeO<sub>2</sub>NPs catalyst was very stable and active, demonstrating that it is appropriate for use in photodegradation reactions.

## ■ CONCLUSION

Synthesis of CeO<sub>2</sub>NPs from *Moringa oleifera* leaf extract can be used for the photo-degradation of phenol. The morphology of nanoparticles is spherical, with a

particle size of 18 nm. CeO<sub>2</sub>NPs showed high photo-degradation by percentage degradation of phenol dye is 94.45% in 120 min irradiation time under visible light. Reusability shows stable results in degrading phenol waste so that it has the potential to be used to remove phenol dye.

#### ■ ACKNOWLEDGMENTS

We would like to thank the Center Research and Community Service Sekolah Tinggi Ilmu Kesehatan Syedza Saintika for funding this research with grant number 02/STIKES-SS/PENEL/VIII-2021.

#### ■ AUTHOR CONTRIBUTIONS

Gusliani Eka Putri, Syukri Arief, and Ahmad Hafizullah Ritonga conducted the experiment, Gusliani Eka Putri and Ahmad Hafizullah Ritonga conducted the analysis of XRD, Eliza Arman, Arniat, Rahmi Yovita Yusuf, and Wiya Elsa Fitri, wrote and revised the manuscript. All authors agreed to the final version of this manuscript.

#### ■ REFERENCES

- [1] Adusei, J.K., Agorku, E.S., Voegborlo, R.B., Ampong, F.K., Danu, B.Y., and Amarh, F.A., 2022, Removal of methyl red in aqueous systems using synthesized NaAlg-g-CHIT/nZVI adsorbent, *Sci. Afr.*, 17, e01273.
- [2] Shu, Z., Zhang, Y., Ouyang, J., and Yang, H., 2017, Characterization and synergetic antibacterial properties of ZnO and CeO<sub>2</sub> supported by halloysite, *Appl. Surf. Sci.*, 420, 833–838.
- [3] Mohamed, A., Abuarab, M.E., Mehawed, H.S., and Kasem, M.A., 2021, Water footprint as a tool of water resources management - Review, *Egypt. J. Chem.*, 64 (12), 7231–7237.
- [4] Prince, J., Tzompantzi, F., Mendoza-Damián, G., Hernández-Beltrán, F., and Valente, J.S., 2015, Photocatalytic degradation of phenol by semiconducting mixed oxides derived from Zn(Ga)Al layered double hydroxides, *Appl. Catal., B*, 163, 352–360.
- [5] Ahmad, T., Iqbal, J., Bustam, M.A., Zulfiqar, M., Muhammad, N., Al Hajeri, B.M., Irfan, M., Anwaar Asghar, H.M., and Ullah, S., 2020, Phytosynthesis of cerium oxide nanoparticles and investigation of their photocatalytic potential for degradation of phenol under visible light, *J. Mol. Struct.*, 1217, 128292.
- [6] Shukla, S.S., Dorris, K.L., and Chikkaveeraiah, B.V., 2009, Photocatalytic degradation of 2,4-dinitrophenol, *J. Hazard. Mater.*, 164 (1), 310–314.
- [7] Ibrahim, M.A., Helmy, E.M., Nazawi, A.M.A., Sadek, M.W., and Abdelatif, M.S., 2021, Biodegradation of nonylphenol ethoxylate in wastewater by *Penicillium chrysogenum*, *Egypt. J. Chem.*, 64 (12), 7251–7262.
- [8] de Elguea-Culebras, G.O., Bravo, E.M., and Sánchez-Vioque, R., 2022, Potential sources and methodologies for the recovery of phenolic compounds from distillation residues of Mediterranean aromatic plants. An approach to the valuation of by-products of the essential oil market – A review, *Ind. Crops Prod.*, 175, 114261.
- [9] Afshar Mogaddam, M.R., Farajzadeh, M.A., Tuzen, M., Jouyban, A., and Khandaghi, J., 2021, Organic solvent-free elevated temperature liquid–liquid extraction combined with a new switchable deep eutectic solvent-based dispersive liquid–liquid microextraction of three phenolic antioxidants from oil samples, *Microchem. J.*, 168, 106433.
- [10] Gamonchuang, J., and Burakham, R., 2021, Amino-based magneto-polymeric-modified mixed iron hydroxides for magnetic solid phase extraction of phenol residues in environmental samples, *J. Chromatogr. A*, 1643, 462071.
- [11] Gong, Y., Ding, P., Xu, M.J., Zhang, C.M., Xing, K., and Qin, S., 2021, Biodegradation of phenol by a halotolerant versatile yeast *Candida tropicalis* SDP-1 in wastewater and soil under high salinity conditions, *J. Environ. Manage.*, 289, 112525.
- [12] Parisi, F., Lazzara, G., Merli, M., Milioto, S., Princivalle, F., and Sciascia, L., 2019, Simultaneous removal and recovery of metal ions and dyes from wastewater through montmorillonite clay mineral, *Nanomaterials*, 9 (12), 1699.
- [13] Ciobanu, C.S., Popa, C.L., and Predoi, D., 2016, Cerium-doped hydroxyapatite nanoparticles synthesized by the co-precipitation method, *J. Serb. Chem. Soc.*, 81 (4), 433–446.

- [14] Sánchez-Rodríguez, D., Méndez Medrano, M.G., Remita, H., and Escobar-Barrios, V., 2018, Photocatalytic properties of BiOCl-TiO<sub>2</sub> composites for phenol photodegradation, *J. Environ. Chem. Eng.*, 6 (2), 1601–1612.
- [15] Handani, S., Emriadi, Dahlan, D., and Arief, S., 2020, Enhanced structural, optical and morphological properties of ZnO thin film using green chemical approach, *Vacuum*, 179, 109513.
- [16] Feng, C., Chen, Z., Jing, J., and Hou, J., 2020, The photocatalytic phenol degradation mechanism of Ag-modified ZnO nanorods, *J. Mater. Chem. C*, 8 (9), 3000–3009.
- [17] Putri, G.E., Rilda, Y., Syukri, S., Labanni, A., and Arief, S., 2021, Highly antimicrobial activity of cerium oxide nanoparticles synthesized using *Moringa oleifera* leaf extract by a rapid green precipitation method, *J. Mater. Res. Technol.*, 15, 2355–2364.
- [18] Putri, G.E., Rilda, Y., Syukri, S., Labanni, A., and Arief, S., 2022, Enhancing morphological and optical properties of montmorillonite/chitosan-modified cerium oxide nanoparticles for antimicrobial applications, *Surf. Interfaces*, 32, 102166.
- [19] Putri, G.E., Arief, S., Jamarun, N., Gusti, F.R., and Fisli, A., 2019, High performance of photocatalytic activity of cerium doped silica mesoporous operating under visible light irradiation, *KnE Eng.*, 4 (2), 128–140.
- [20] Kumar, S., Tripathy, S., Singh, O.K., and Singh, S.G., 2021, Cerium oxide nanofiber based electroanalytical sensor for TNF- $\alpha$  detection: Improved interfacial stability with Nafion, *Bioelectrochemistry*, 138, 107725.
- [21] Onoda, H., and Tanaka, R., 2019, Synthesis of cerium phosphate white pigments from cerium carbonate for cosmetics, *J. Mater. Res. Technol.*, 8 (6), 5524–5528.
- [22] Caputo, F., Mameli, M., Sienkiewicz, A., Licoccia, S., Stellacci, F., Ghibelli, L., and Traversa, E., 2017, A novel synthetic approach of cerium oxide nanoparticles with improved biomedical activity, *Sci. Rep.*, 7 (1), 4636.
- [23] Bui, H.T., Weon, S., Bae, J.W., Kim, E.J., Kim, B., Ahn, Y.Y., Kim, K., Lee, H., and Kim, W., 2021, Oxygen vacancy engineering of cerium oxide for the selective photocatalytic oxidation of aromatic pollutants, *J. Hazard. Mater.*, 404, 123976.
- [24] Radić, N., Grbić, B., Petrović, S., Stojadinović, S., Tadić, N., and Stefanov, P., 2020, Effect of cerium oxide doping on the photocatalytic properties of rutile TiO<sub>2</sub> films prepared by spray pyrolysis, *Phys. B*, 599, 412544.
- [25] Putri, G.E., Gusti, F.R., Sary, A.N., Arief, S., Jamarun, N., and Amar B, S., 2019, Synthesis and antimicrobial activity of cerium oxide/AG dopes silica mesoporous modification as nanofillers for food packaging applications, *Malays. Appl. Biol.*, 48 (4), 25–32.
- [26] Feng, N., Liu, Y., Dai, X., Wang, Y., Guo, Q., and Li, Q., 2022, Advanced applications of cerium oxide based nanozymes in cancer, *RSC Adv.*, 12 (3), 1486–1493.
- [27] Arumugam, A., Karthikeyan, C., Haja Hameed, A.S., Gopinath, K., Gowri, S., and Karthika, V., 2015, Synthesis of cerium oxide nanoparticles using *Gloriosa superba* L. leaf extract and their structural, optical and antibacterial properties, *Mater. Sci. Eng., C*, 49, 408–415.
- [28] Singh, K.R.B., Nayak, V., Sarkar, T., and Singh, R.P., 2020, Cerium oxide nanoparticles: Properties, biosynthesis and biomedical application, *RSC Adv.*, 10 (45), 27194–27214.
- [29] Arunachalam, T., Karpagasundaram, U., and Rajarathinam, N., 2017, Ultrasound assisted green synthesis of cerium oxide nanoparticles using *Prosopis juliflora* leaf extract and their structural, optical and antibacterial properties, *Mater. Sci.-Pol.*, 35 (4), 791–798.
- [30] Muthuvel, A., Jothibas, M., Mohana, V., and Manoharan, C., 2020, Green synthesis of cerium oxide nanoparticles using *Calotropis procera* flower extract and their photocatalytic degradation and antibacterial activity, *Inorg. Chem. Commun.*, 119, 108086.

- [31] Fan, Y., Li, P., Hu, B., Liu, T., Huang, Z., Shan, C., Cao, J., Cheng, B., Liu, W., and Tang, Y., 2019, A smart photosensitizer-cerium oxide nanoprobe for highly selective and efficient photodynamic therapy, *Inorg. Chem.*, 58 (11), 7295–7302.
- [32] Zamri, M.S.F.A., and Sapawe, N., 2019, Kinetic study on photocatalytic degradation of phenol using green electrosynthesized TiO<sub>2</sub> nanoparticles, *Mater. Today: Proc.*, 19, 1261–1266.
- [33] Pathak, T.K., Coetsee-Hugo, E., Swart, H.C., Swart, C.W., and Kroon, R.E., 2020, Preparation and characterization of Ce doped ZnO nanomaterial for photocatalytic and biological applications, *Mater. Sci. Eng., B*, 261, 114780.
- [34] Scott, T., Zhao, H., Deng, W., Feng, X., and Li, Y., 2019, Photocatalytic degradation of phenol in water under simulated sunlight by an ultrathin MgO coated Ag/TiO<sub>2</sub> nanocomposite, *Chemosphere*, 216, 1–8.
- [35] Fujishima, A., Zhang, X., and Tryk, D.A., 2008, TiO<sub>2</sub> photocatalysis and related surface phenomena, *Surf. Sci. Rep.*, 63 (12), 515–582.
- [36] Liu, J., Wang, H., Chang, M.J., Sun, M., Zhang, C.M., Yang, L.Q., Du, H.L., and Luo, Z.M., 2022, Facile synthesis of BiOCl with extremely superior visible light photocatalytic activity synergistically enhanced by Co doping and oxygen vacancies, *Sep. Purif. Technol.*, 301, 121953.
- [37] Thulasinathan, B., Jayabalan, T., Arumugam, N., Rasu Kulanthaisamy, M., Kim, W., Kumar, P., Govarthan, M., and Alagarsamy, A., 2022, Wastewater substrates in microbial fuel cell systems for carbon-neutral bioelectricity generation: An overview, *Fuel*, 317, 123369.
- [38] AlSalhi, M.S., Devanesan, S., Asemi, N., and Ahamed, A., 2023, Concurrent fabrication of ZnO–ZnFe<sub>2</sub>O<sub>4</sub> hybrid nanocomposite for enhancing photocatalytic degradation of organic pollutants and its bacterial inactivation, *Chemosphere*, 318, 137928.
- [39] Karimi-Maleh, H., Kumar, B.G., Rajendran, S., Qin, J., Vadivel, S., Durgalakshmi, D., Gracia, F., Soto-Moscoso, M., Orooji, Y., and Karimi, F., 2020, Tuning of metal oxides photocatalytic performance using Ag nanoparticles integration, *J. Mol. Liq.*, 314, 113588.
- [40] Guan, X., Zhang, R., Jia, B., Liu, G., Yan, B., Lu, P., and Peng, G.D., 2022, Influence of ring structures on luminescence properties of trivalent cerium in Ge-doped silica optical fiber, *J. Non-Cryst. Solids*, 576, 121251.
- [41] Orooji, Y., Tanhaei, B., Ayati, A., Tabrizi, S.H., Alizadeh, M., Bamoharram, F.F., Karimi, F., Salmanpour, S., Rouhi, J., Afshar, S., Sillanpää, M., Darabi, R., and Karimi-Maleh, H., 2021, Heterogeneous UV-switchable Au nanoparticles decorated tungstophosphoric acid/TiO<sub>2</sub> for efficient photocatalytic degradation process, *Chemosphere*, 281, 130795.